Effect of airfoil profile on aerodynamic performance and economic assessment of H-rotor vertical axis wind turbines

Jafari, Mohammad ; Razavi, Alireza ; Hosseini, Seyed Mojtaba Mir

Published in:
Energy

DOI (link to publication from Publisher):
10.1016/j.energy.2018.09.124

Publication date:
2018

Document Version
Accepted author manuscript, peer reviewed version

Accepted Manuscript

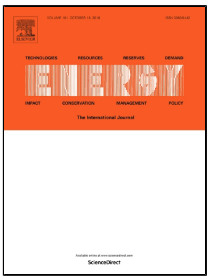

Effect of Airfoil Profile on Aerodynamic Performance and Economic Assessment of H-rotor Vertical Axis Wind Turbines

Mohammad Jafari, Alireza Razavi, Mojtaba Mirhosseini

PII:	S0360-5442(18)31888-7
DOI:	10.1016/j.energy.2018.09.124
Reference:	EGY 13818
To appear in:	*Energy*
Received Date:	17 January 2018
Accepted Date:	18 September 2018

Please cite this article as: Mohammad Jafari, Alireza Razavi, Mojtaba Mirhosseini, Effect of Airfoil Profile on Aerodynamic Performance and Economic Assessment of H-rotor Vertical Axis Wind Turbines, *Energy* (2018), doi: 10.1016/j.energy.2018.09.124

Effect of Airfoil Profile on Aerodynamic Performance and Economic Assessment of H-rotor Vertical Axis Wind Turbines

Mohammad Jafari [a], Alireza Razavi [a], Mojtaba Mirhosseini [b,*]

[a] Aerospace Engineering Department, Iowa State University, Ames, IA 50011, USA
[b] Department of Energy Technology, Aalborg University, Pontoppidanstraede 111, 9220 Aalborg East, Denmark

*Corresponding author: seh@et.aau.dk

ABSTRACT

This research focuses on the effects of the asymmetric airfoil profiles on aerodynamic performance and economic evolution of a vertical axis wind turbine (VAWT) at different blade heights, solidities, and tip speed ratios (TSR or λ). The aerodynamic performance of six asymmetric airfoils, S809, S814, RISØ-A1-24, Du 93-W-210, FFA-W3-241, and FX66-S196-V1, was calculated using double multiple-stream tube (DMST) theory and blade element methods for determination of their performance for tip speed ratios from 1 to 12, and solidities of 0.2 to 0.6, were considered for this study. All calculations focused on the Khaf area (rural zone) in Iran and considered two heights: 10 m and 40 m. To verify the performance of the developed code, results were compared with experimental power coefficient data for NACA0012 airfoil. For FFA-W3-241 airfoil, maximum power coefficient was obtained at solidity of 0.5 and tip-speed ratio of 4.This aerodynamic excellence resulted in 22.4% and 21.9% increase in annual energy production at hub heights (h) of 10 m and 40 m, respectively, while keeping the total investment costs constant. Moreover, the ratio of wind-generated electric power sales to the total investment cost was found to be 4.33 (0.15/0.0346) for 15 years of operation.

Keywords: H-type Vertical Axis Wind Turbine; Double Multiple Stream Tube (DMST) Model; Blade Element Momentum Theory; Airfoil Selection; Power Generation; Economic Evaluation.

1. Introduction

National economic growth is highly dependent on energy consumption. Until 1973 and oil price crisis, fossil fuels were the main source of energy. In 1974, the U.S. government initiated a project with industry to develop commercial wind turbines. Introduction of the MOD-5B was one outcome of the project which was the largest single rotor wind turbine in 1987, with a rotor span of about 100 m and a power capacity of 3.2 MW. At the same time, Denmark began the development of multi-megawatt wind turbines and

introduced the first multi-megawatt wind turbine in 1978. Nowadays, utilization of fossil fuels has become more restricted due to the global warming, price fluctuations, and decline in reservoirs [1], while at the same time energy consumption has increased rapidly around the world. The U.S. Energy Information Administration (EIA) has predicted a 28% increase in international energy consumption by 2040 [2]. These contradictory events highlight the need for improvement in the energy harvest from environment-friendly sources, especially wind. Both rotary and bladeless turbine systems [3] can be used to extract wind energy, and while the bladeless systems are not as common, both Horizontal Axis Wind Turbines (HAWT) and Vertical Axis Wind Turbines (VAWT) are widely used. In general, VAWTs have several advantages over HAWTs, including lower noise pollution, no need for yaw mechanisms, installation of the generator at lower elevations, independence to wind direction, and ease of manufacturing and maintenance [4, 5]. These features make them an interesting choice, especially for off-grid and small-scale energy production [4, 6].

Power extraction in VAWTs is based on either lift or drag forces which divides the VAWTs into two types: Darrieus and Savonius. Since the Darrieus VAWT, the lift-based configuration, has higher coefficients of power, it is more commonly used. Based on blade configuration, there are generally two types of Darrieus VAWTs: (a) curved-blade and (b) straight-blade [7]. Achievement of high power coefficient, ease of construction and operation, and manufacturing cost are important factors in selection of VAWTs for power production, so straight-line blades, especially the H-rotor types, have become more popular due to their manufacturing simplicity [8].

Increasing the power coefficient of VAWTs will reduce the cost of power generation. For this purpose, three important parameters of solidity, tip-speed ratio (TSR), and blade profile were studied to facilitate prediction and optimization of aerodynamic forces [9, 10]. These aerodynamic forces can be estimated from the lift and drag coefficients of each airfoil. Aerodynamic performance of VAWTs has been investigated both numerically [4, 11-15] and experimentally [8, 11, 14, 16-19]. Singh, et al., [8] studied the effect of rotor solidity at different wind speeds on the performance of a three-bladed H-type Darrieus rotor with asymmetrical S1210 blades. It was found that high solidity improves the power coefficient and the performance of VAWTs in general. They also found the optimum magnitude of rotor solidity for the specified mean wind speed at the site. In 2017, Qamar and Janajreh [4], investigated the effect of solidity for Darrieus VAWTs and confirmed Singh, et al.'s [8] conclusion that there is an optimum solidity where the coefficient of performance reaches the maximum value for a given mean wind speed. Subramanian, et al., [18] numerically studied the effect of different NACA airfoils on the performance of VAWTs and found that different airfoils perform differently for various tip-speed ratios; thicker airfoils perform better for low tip-speed ratios because of the long duration of the attached flow,

while thinner airfoils work better for higher tip-speed ratios since they dissipate the vortex shedding faster. One problem of VAWTs is their relative high turbulence on a turbine's leeward side, which is induced by the windward interaction between the turbine blades and freestream wind. To study the effect of this phenomena on the cost of power generation, Brulle [19] compared the performance of VAWT and HAWT using the same airfoils and a constant mean free-stream velocity. A variable pitch VAWT with 500 kW capacity demonstrated an 18% reduction in the cost of power generation when compared to a HAWT at a mean wind speed of 5.4 m/s. Mohamed [20] used 2D-CFD simulations to study the effect of symmetric and asymmetric airfoils on power coefficient of a H-rotor Darrieus VAWT and found that use of the asymmetric S-1046 airfoil improves the output power by 26.83% compared to that of a symmetric NACA airfoil. Sengupta, et al., [21] confirmed Mohamed's [20] conclusions on improvement of power coefficient using asymmetrical rather than symmetrical airfoils at low wind speeds (4 m/s to 8 m/s). Saeidi, et al., [1] investigated the effects of solidity and tip-speed ratio on power coefficient and economic feasibility for a 3-bladed H-type Darrieus rotor with a NACA 4415 airfoil. They found that the maximum power coefficient of 0.47 occurred at solidity of 0.4 and tip-speed ratio of 4. They also observed a reduction of 50% in cost of electricity generation at the maximum power coefficient. In their study, the effect of aerodynamic airfoil performance on cost of the electricity was not considered. Chen, et al., [22] numerically investigated effects of three design parameters of a NACA 4-digit-modified airfoil on the power coefficient of lift-type VAWTs: thickness-to-chord ratio, leading-edge radius, and maximum thickness expressed in tenths of chord. They found that the thickness-to-chord ratio has the biggest influence on power coefficient and the optimum tip-speed ratio varies with the airfoil design. Ma, et al., [23] focused on optimization of airfoils to improve the power performance of a three-blade high-solidity VAWT. By coupling the genetic algorithm with CFD simulations, they were able to improve the power coefficient by up to 26.82%. Bukala et al. [24] showed that for small wind turbines, initial cost to annual energy output ratio of VAWTs is less than 0.04 which is much worse than the standard and shrouded VAWTs which average about 0.16. Very low efficiency and system costs were the reason of this performance which urges for increase in the efficiency of VAWTs. In addition to optimization of power coefficient in wind turbines, cost estimation, i.e., cost per kWh of energy in lifetime of the wind turbines is important. Obviously, energy production using vertical axis wind turbines should be economical to compete other methods. Cost of the onshore power generation in the United States reduced from about \$0.3/kWh to about \$0.055/kWh [25]. A report by Cleantechnica [26] showed that total cost of wind generation in high wind resource areas (United States, Brasil, Mexico, Sweden) was below \$0.068/kWh, which could compete the total costs of coal-fired and gas-fired power as \$0.067/kWh and \$0.056/kWh, respectively. Further decrease in this price can make the wind power generation even more competitive. U.S. Energy Information Administration (EIA) updated the total cost of electricity in 2017 [27] where

onshore wind power cost was $0.037/kWh, cheaper than any other methods of power generation. Further increase in this pricing, makes the wind energy even more desirable.

In the present work, effects of asymmetric airfoils, i.e., S809, S814, RISØ-A1-24, DU 93-W-210, FFA-W3-241, FX66-S196-V1, on design of wind turbine blades, specifically the aerodynamic performance of a H-rotor VAWT in terms of power coefficient were studied. To evaluate the effect of blade section only, different solidities and tip speed ratios were considered, while other parameters such as the turbine height (H), number of blades (N), and chord length (c) were kept fixed. The double multiple stream tube (DMST) model, with extensive use in the literature for analyze the performance of vertical axis wind turbines was used. History of this method begins with Templin's [28] introduction of the single stream tube model based on the BEM method. Paraschivoiu [29] then modified the model to DMST so it could predict the performance of Darrieus wind turbines more accurately. In 2005, Coiro, et al., [30] investigated the accuracy of the DMST model by comparison with experimental results and concluded that it can predict both static and dynamic performance of vertical axis wind turbines, especially for solidities less than or equal to 0.5. In this research, effect of dynamic stall is not considered because predicting dynamic stall response is significantly more challenging, and it also depends on many additional parameters such as blade profile, rate of the change of the angle of attack, turbulence level, type of the motion, and three-dimensional effects. Moreover, past studies showed that the most of dynamic stall's effects shows up in low tip speed ratios, while the main focus of this research is on maximum power coefficient which all happened at high tip speed ratios where dynamic stall has negligible effects. To validate the results of this research, results of the developed code were compared with the experimental data of NACA0012 and the numerical results (using DMST) of NACA4415, and the values for power coefficients and tangential forces showed a good agreement. After studying the aerodynamic performance of all airfoils, economic evaluation was carried out to reveal the effect of airfoil selection on annual energy production and manufacturing costs, including installation, operation, and maintenance.

2. Aerodynamic model description

In this study, the DMST model was used to study the effects of the aerodynamic characteristics of six different airfoils on performance of a H-rotor VAWT turbine. Although this method does not consider the dynamic stall, past studies have shown that the dynamic stall condition usually occurs at low tip-speed ratios and is more significant in non-straight blade VAWTs [31-33]. Since only a straight blade (H-type) was used in this research, and only Cp_{max} was important for cost evaluation of all airfoils, this method was

selected for the performance prediction. In the DMST model, flow around the rotor is divided into the upstream ($\frac{-\pi}{2} < \theta < \frac{\pi}{2}$) and downstream ($\frac{\pi}{2} < \theta < \frac{3\pi}{2}$) regions and passes through two tubes located at each region with an embedded actuator disk (Fig. 1) that result in a pressure drop in the flow field only at the location of the disks. One-dimensional momentum theory was applied to relate the upstream and downstream velocities. Three velocities were defined inside the domain (Fig. 1), all related to the free-stream velocity through the definitions of induction factors at upstream and downstream regions as shown in Eqs. (1-3) [1, 29, 34].

$$V = uV_\infty \tag{1}$$

$$V_e = (2u-1)V_\infty \tag{2}$$

$$V' = u'(2u-1)V_\infty \tag{3}$$

where u and u' are induction factors of the upstream and downstream sections, respectively.

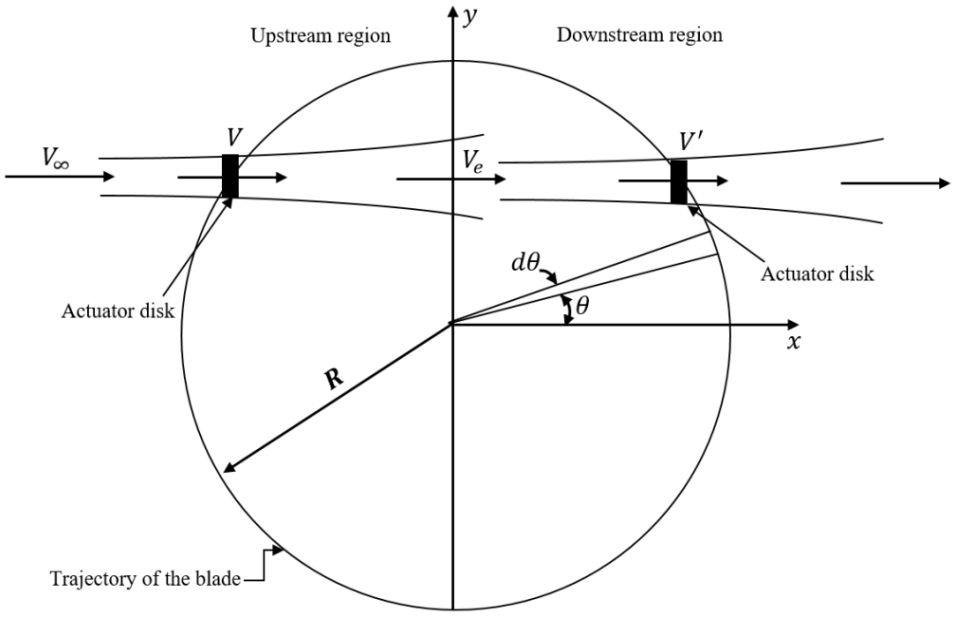

Fig. 1: Description of upstream and downstream domain in DMST.

To calculate these induction factors, the blade-element method was combined with the momentum theory [29, 34], where an iterative approach with a residual of 10^{-4} was used to solve the equations (Fig. 2). The initial value of the upstream induction factor was considered equal to 1.

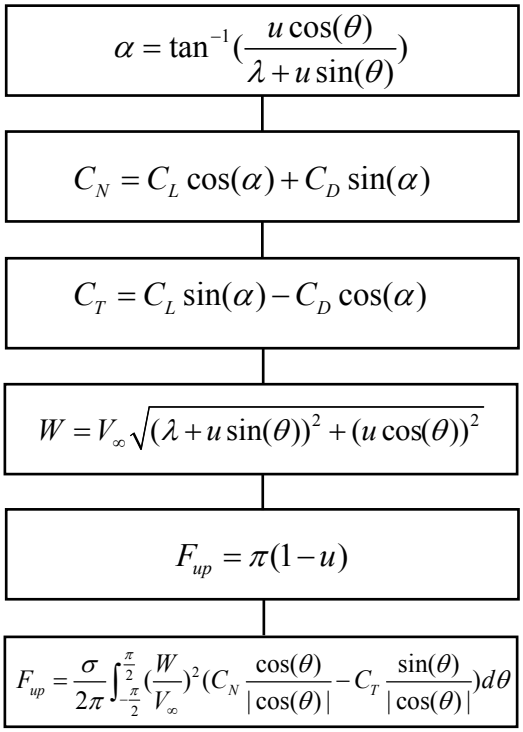

Fig. 2: Flow chart of the iterative approach to calculate the upstream induction factor.

In Fig. 2, α is the angle of attack, $\lambda = \frac{R\omega}{V_\infty}$ is the local tip-speed ratio, u is induction factor, V_∞ is upstream wind speed, R is the radius of wind turbine rotor, ω is the angular velocity of the rotor, θ is the azimuth angle (Fig. 3), σ is the solidity factor defined as ($\sigma = \frac{Nc}{R}$), N is the number of blades, and c is the blade chord. C_T and C_N are non-dimensional normal and tangential force coefficients, respectively (see Fig. 2). Drag (C_D) and lift (C_L) coefficients were extracted from the results in ref. [35]. W is local relative wind speed in upstream region, and F_{up} is upwind function.

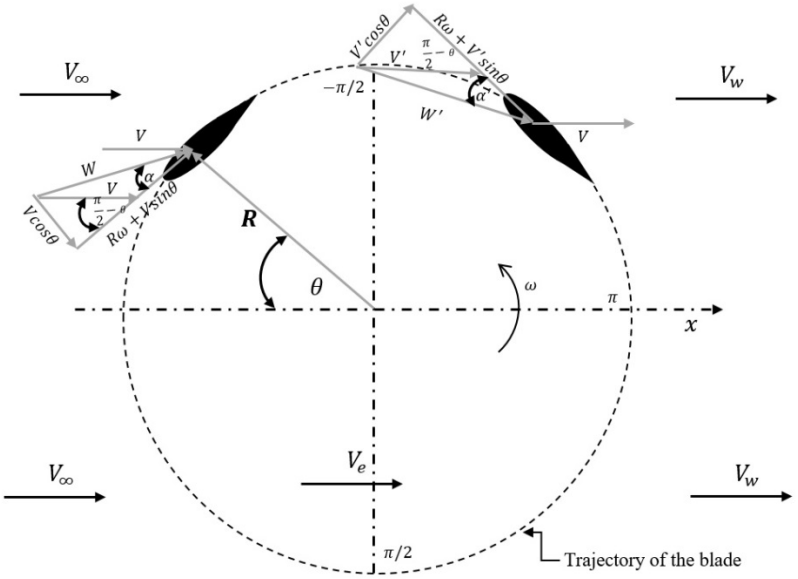

Fig. 3: Schematic view of wind speed vectors in upstream and downstream of the VAWT.

In this study, normal (F_N) and tangential (F_T) forces are functions of azimuth angle (θ) and are shown in Fig. 4 that can be calculated using Eqs. 4 and 5:

$$F_N(\theta) = \frac{A_P}{A_S} C_N \left(\frac{W}{V_\infty}\right)^2 \tag{4}$$

$$F_T(\theta) = \frac{A_P}{A_S} C_T \left(\frac{W}{V_\infty}\right)^2 \tag{5}$$

where $A_S = 2\pi RH$ is the rotor sweep area, H is the blade height, and the blade projection area is defined as $A_P = cH$. To perform a better comparison, tangential and normal forces were normalized with $0.5\rho A_P V_\infty^2$. In Fig. 4, procedure of force components decomposition is adapted from [36].

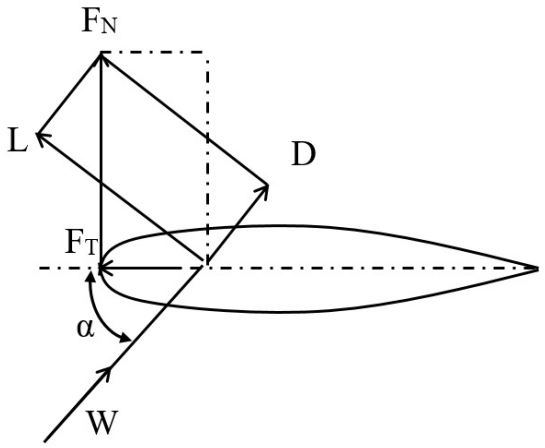

Fig. 4: Aerodynamic forces on an airfoil section.

The power coefficient for the upstream region was defined as:

$$\bar{C}_{Pup} = \frac{\sigma}{4\pi}\int_{-\frac{\pi}{2}}^{\frac{\pi}{2}} C_T \left(\frac{W}{V_\infty}\right)^2 d\theta \tag{6}$$

$$C_{Pup} = \lambda.\bar{C}_{Pup} \tag{7}$$

where ($\bar{C}_{Pup}$) is the mean upwind power coefficient and (C_{Pup}) is the upwind power coefficient.

To determine the same parameters for the downstream (indexed by dw) region, an iterative approach as shown in Fig. 5 was used [1, 29, 34], and downstream parameters were designated with a prime symbol " ′ ". Definition of all variables in Fig. 5 similar to Fig. 2.

Normal ($F_N'(\theta)$), and tangential components ($F_T'(\theta)$) of the resultant forces were calculated using:

$$F_N'(\theta) = \frac{A_P}{A_S} C_N' \left(\frac{W'}{V_\infty}\right)^2 \tag{8}$$

$$F_T'(\theta) = \frac{A_P}{A_S} C_T' \left(\frac{W'}{V_\infty}\right)^2 \tag{9}$$

The contribution of the downstream flow to the power coefficient was:

$$\bar{C}_{Pdw}(\theta) = \frac{\sigma}{4\pi}\int_{\frac{\pi}{2}}^{\frac{3\pi}{2}} C_T' \left(\frac{W'}{V_\infty}\right)^2 (d\theta) \tag{10}$$

$$C_{Pdw}(\theta) = \lambda.\bar{C}_{Pdw} \tag{11}$$

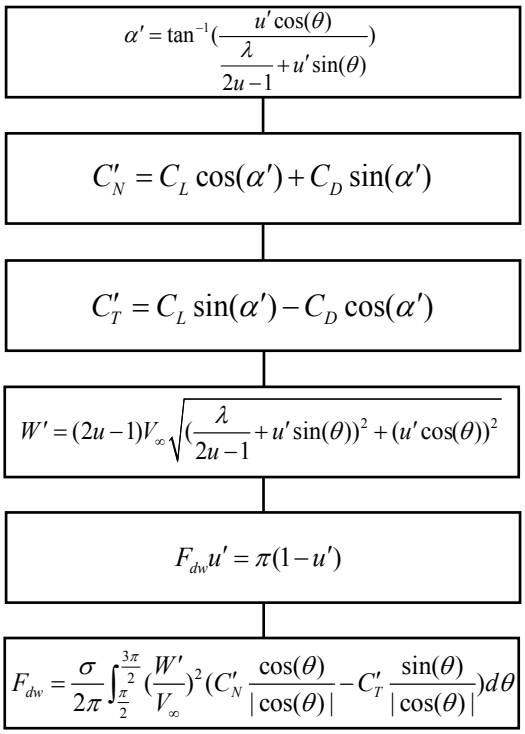

Fig. 5: Flow chart of the iterative approach to calculate the downstream induction factor.

Finally, the power coefficients of upstream and downstream regions were added to find the total power coefficient as follows:

3. Code validation

To validate the developed code that was written in MATLAB, experimental results of the power coefficient [37] were compared with the numerical results of the current study for the NACA0012 airfoil at Re=360000 and a solidity of 0.18 (Fig. 6). The comparison shows a good agreement between the results. In addition, a comparison was made with another numerical study [1] that used the same method for investigation on NACA4415. Solidity and tip-speed ratio were considered 0.4 of 4, respectively. As shown in Fig. 7, while a good match between the results of the current and previous numerical study for the same airfoil profile was observed, there are some differences between the two numerical solutions for high tip-speed ratios due to use of different approaches for fitting the C_D and C_L equation (13, 14) curves as functions of the angle of attack. These two verification steps indicated that the present code can provide a good prediction of aerodynamic performance for different airfoil profiles.

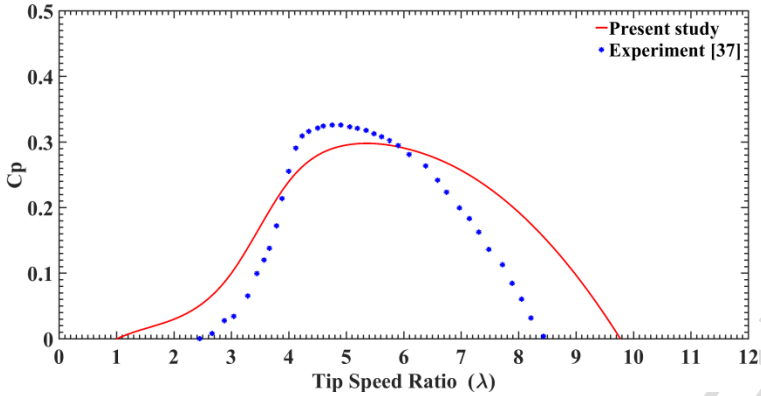

Fig. 6: Comparison of power coefficient for NACA0012 between the present study and the experimental data [37] at $\sigma = 0.18$ and Re=360000.

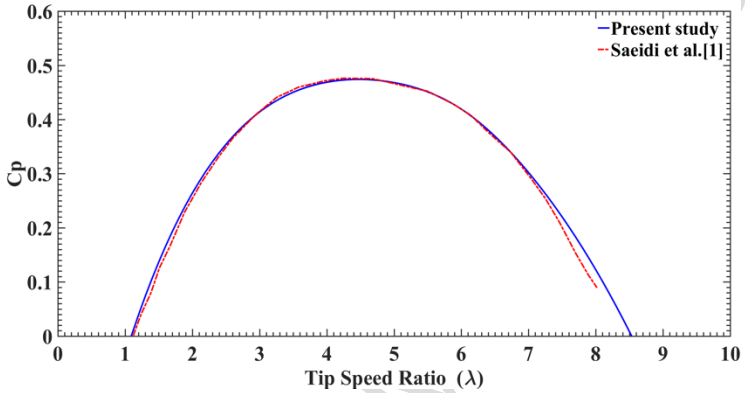

Fig. 7: Validation of present study for NACA 4415 with the results from another numerical study [1] at $\sigma = 0.4$ and λ=4.

4. Airfoil properties

In this study, six common airfoil profiles for HAWTs were obtained from XFOIL code [35] both for investigation of aerodynamic performance and economic evaluation in design of VAWTs. XFOIL code is based on a combination of a panel method and assumption of a viscous boundary layer. The main reason for the selection of current airfoil profiles for the design of the H-type VAWT was their relative high lift-to-drag ratio. Even though these are well-known airfoils for horizontal axis wind turbines, its desirable to study their application and influence on vertical axis wind turbines and its performance and aerodynamic features. Lift and drag coefficients of the airfoils, that are functions of the angle of attack, were fitted with polynomials of degree 3 or less, although for some airfoils, two separate equations for either C_L or C_D were required over the whole range of the angles of attacks (α_s) to provide a more precise curve-fitting. The separating point between the two equations is defined as α_s in Table 1. Equations 13 and 14 define the lift and drag coefficients as constants. In Table 1, constants that are calculated from the curve-fitting are shown for different airfoils.

$$C_L(\alpha) = a_3\alpha^3 + a_2\alpha^2 + a_1\alpha + a_0 \quad (13)$$

$$C_D(\alpha) = b_3\alpha^3 + b_2\alpha^2 + b_1\alpha + b_0 \quad (14)$$

Table 1
Constants of C_L or C_D equations for all airfoil (R^2>0.99).

Airfoil type	a_3	a_2	a_1	a_0	b_3	b_2	b_1	b_0	α_s^o
S809	0	-15.02	8.101	0.140	2.420	0.292	-0.059	0.011	---
S814	0	-17.01	8.767	0.357	5.865	-1.13	0.073	0.009	---
RISØ-A1-24	0	0	6.737	0.434	0	0.126	0.004	0.008	<11
	-108	111.22	-37.76	5.632	0	0	0.971	-0.172	>11
DU 93-W-210	26.46	-29.57	10.21	0.404	2.562	0.320	-0.074	0.011	---
FFA-W3-241	-24.44	-3.901	8.145	0.264	0	0.164	0.002	0.007	<11
					0	3.056	-0.956	0.076	>11
FX66-S196-V1	0	0	6.731	0.531	-1.008	0.229	0.003	0.007	<8
	-100.1	81.47	-21.08	3.170	0	0	0.612	-0.082	>8

5. Wind characteristics

To be consistent with the reported data from the wind energy potential assessment in Iran [38], the Khaf area with the highest annual mean wind speed [38] was selected for mounting the H-rotor VAWT. In Table 2, mean wind speed, shape factor, and scale factor for the Weibull distribution of wind in this area are provided at heights of 10 m, 30 m, and 40 m [38], while in the economic evaluation, the annual energy production and the economic comparison were made only for the heights of 10 m and 40 m.

Table 2
Wind characteristics of Khaf area (Iran).

	Height (m)		
	10	30	40
Mean wind speed (m/s)	9.208	10.439	10.817
Shape factor for Weibull probability density function, k	1.618	1.611	1.643
Scale factor for Weibull probability density function, c	10.34	11.81	12.48

6. Result and discussion

6.1 Aerodynamic performance

6.1.1 Power coefficient (Cp)

The aerodynamic performance was investigated to determine the best airfoil profile in terms of maximum power coefficient, annual energy production, and minimum investment; the tip-speed ratio was therefore

changed over the range of 1 to 12 (with incremental steps of 0.1) for solidities ranging between 0.2 and 0.6. In Fig. 8, power coefficients were calculated for all airfoils at different solidities and tip-speed ratios. This figure shows that solidity of 0.5 is an optimum point for these airfoils to obtain the maximum power coefficient, and it also shows that Cp curve is wider for lower solidities, and finding an optimum point is in agreement with other studies on VAWTs. Fig. 9 shows that the minimum (0.413) and maximum (0.509) peak power coefficients are associated with S809 and FFA-W3-241, respectively, that occur at $\sigma = 0.5$ and $\lambda=4$. Table 3 provides a summary of design parameters for all airfoils. To study the sole effect of the airfoil profile, other parameters, i.e., the number of blades ($N = 3$), the turbine height ($H = 3$ m), and the chord length ($c = 0.25$ m) were kept constant. The rated power corresponding to the maximum power coefficients of each airfoil was calculated at the rated wind speed of 12 m/s (Table 3) because this wind speed, commonly selected by wind turbine manufacturing companies, is also near the mean wind speed in Khaf. Airfoils S809 and FFA-W3-241 produced the minimum (3.85 kW) and maximum (4.75 kW) rated power magnitudes, respectively. This also reveals that the significant effect of change in the airfoil section can lead to improvement of wind turbine efficiency.

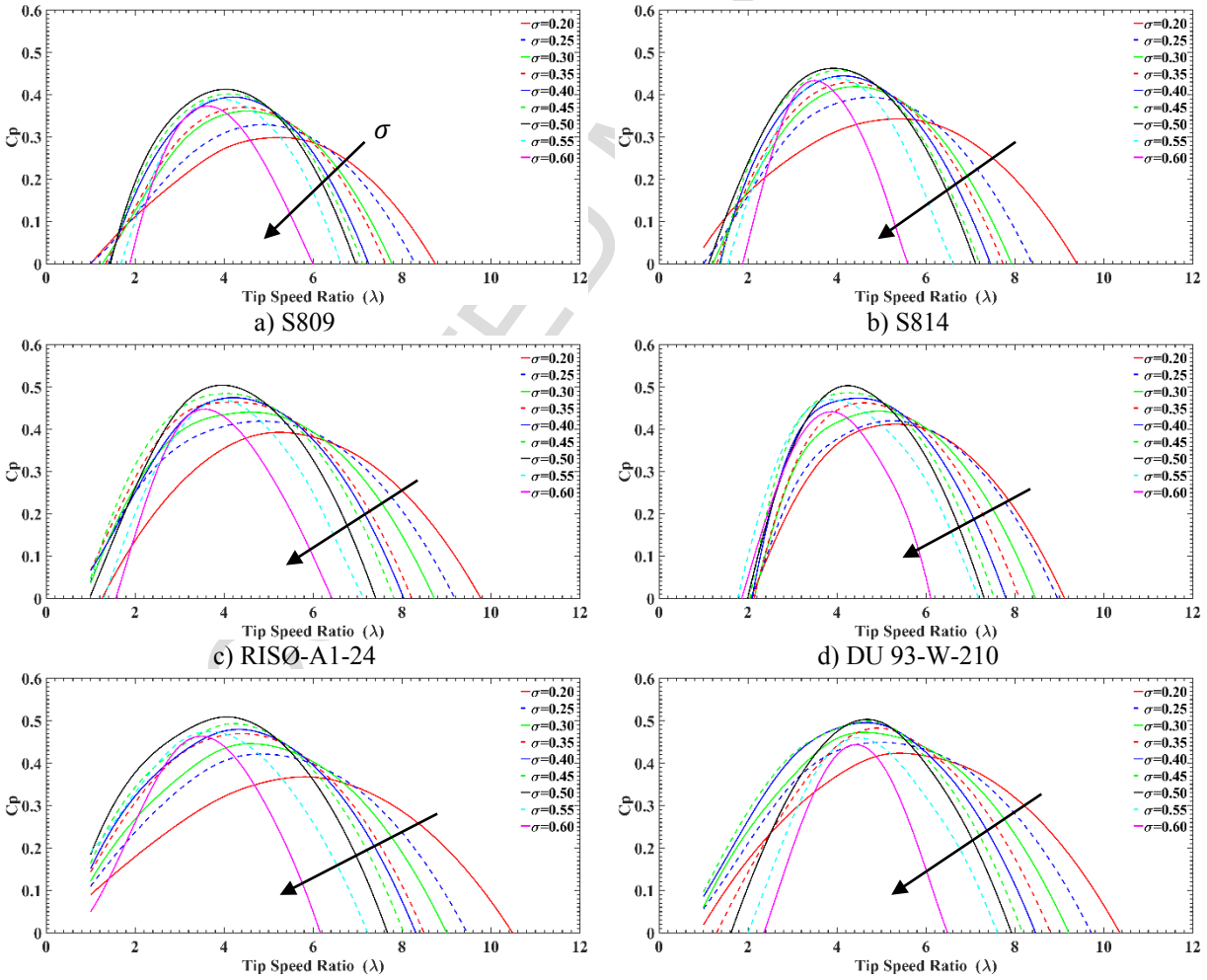

e) FFA-W3-241 f) FX66-S196-V1

Fig. 8: Power coefficient for different airfoils as a function of tip speed ratio at various solidities.

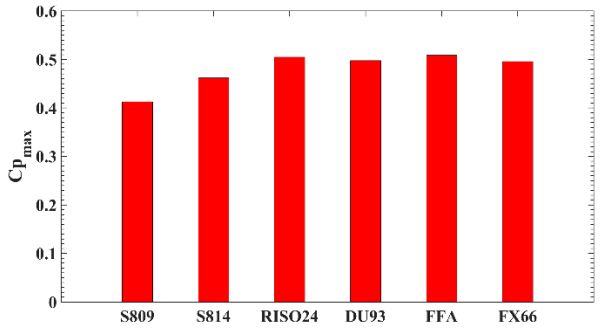

Fig. 9: Comparison of Cp_{max} for different airfoil profiles.

Table 3
Properties of H-type VAWT designed for Khaf area (Iran).

Airfoil type	H (m)	R (m)	c (m)	N	σ	λ	Cp_{max}	Rated Power (kW) $P = 0.5\rho V_{\infty}^{3} 2RHC_{p.max}$
S809	3	1.5	0.25	3	0.5	4	0.413	3.85
S814	3	1.5	0.25	3	0.5	4	0.462	4.31
RISØ-A1-24	3	1.5	0.25	3	0.5	4	0.505	4.71
DU 93-W-210	3	1.5	0.25	3	0.5	4	0.498	4.65
FFA-W3-241	3	1.5	0.25	3	0.5	4	0.509	4.75
FX66-S196-V1	3	1.5	0.25	3	0.5	5	0.496	4.63

6.1.2 Tangential and normal force (F_T & F_N)

The aerodynamic force on a VAWT is highly dependent on the azimuth angle that is related to a large fluid force at the upstream region. Tangential and normal forces of all airfoils are depicted for different solidities of 0.2 to 0.5 and different tip speed ratios in Figs. 10-15. Comparison of normal forces for all cases illustrates that the absolute value of normal force is mostly reduced with decreasing the tip-speed ratio, while a smaller change can be seen in the downstream side (θ =90°~270°). This small change in the downstream region reflects the dominant effect of the wake behind the wind turbine. As shown in Fig. 10, normal force coefficient sometimes becomes slightly negative for downstream region (θ=90º-270º) only at low TSRs and solidities. Normal force (F_N) has negative value when C_N is negative (Eq. 4). This term becomes negative in downstream region when alpha is negative, and, as a result, Sin (α) becomes negative. This happens only when alpha has highest negative value (magnitude-wise), and this condition only occurs in low TSRs and solidities (see Fig. A1-A6). This negative force has been seen commonly in other numerical and experimental studies [39, 40]. It is clear that the tangential force achieves a maximum magnitude because the blade is moving toward the upstream side at azimuth angles between 0° and 30°.

Conversely, the tangential force becomes small and smooth when the blade is moving at azimuth angle between 90° and 270°. The reason for this tendency is mainly considered to be the effect of the absolute attack angle of the blade, larger in the upstream region than in the downstream region. While agreement between different tip-speed ratios is quite good in the upstream region of the rotation area, despite the fact that aerodynamic loading is highest there, some discrepancies can be observed if the azimuth angle is changed during rotation. For symmetric airfoils, peak of the tangential force decreases with an increase in tip-speed ratio where the blade leads to a lower azimuth angle. However, for all the airfoils studied, this trend was not observed, probably because of the asymmetric shapes and types of the airfoils. For the lowest tip-speed ratio in the current study and in the downstream region, DMST anticipates negative normal and tangential forces for some airfoils. Comparison of tangential forces demonstrates that the effect of changing the solidity and tip speed ratio is significant in some cases, including RISØ-A1-24, FFA-W3-241 and FX66-S196-V1, but is insignificant in other cases of S809, S814, and DU 93-W-210.

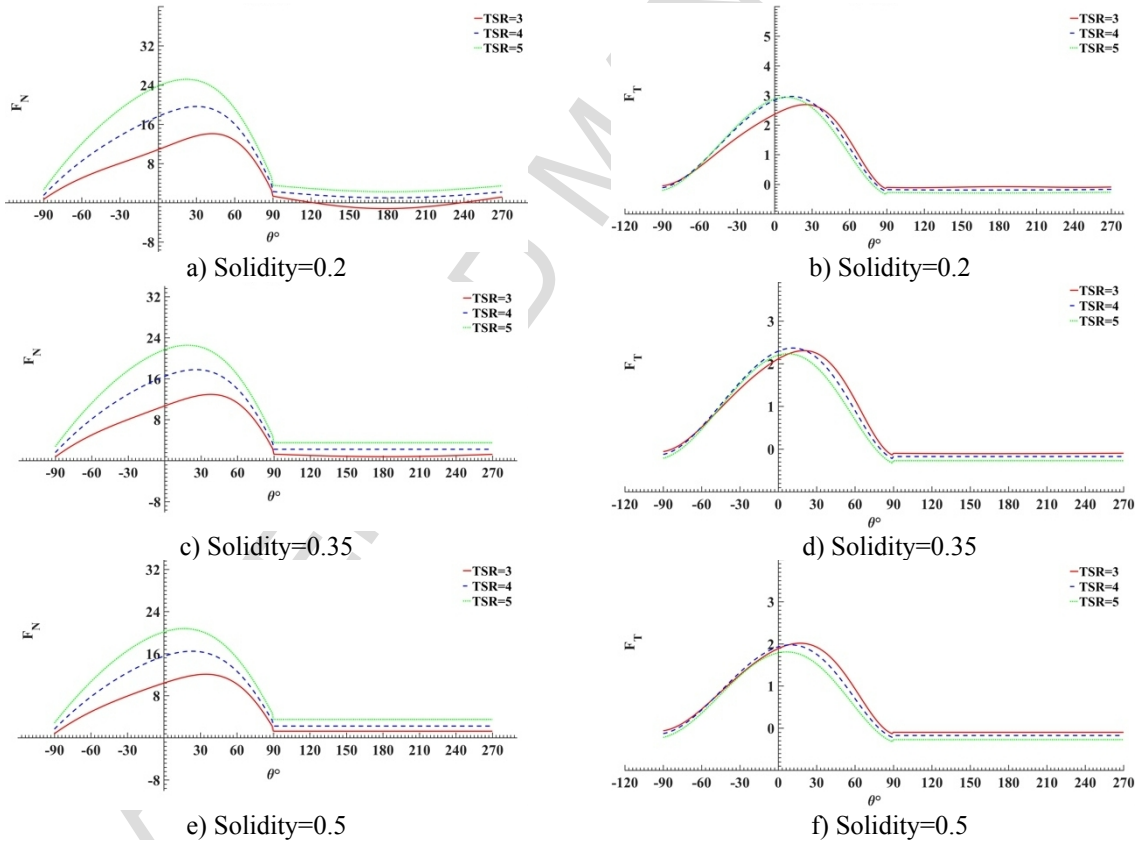

a) Solidity=0.2 b) Solidity=0.2

c) Solidity=0.35 d) Solidity=0.35

e) Solidity=0.5 f) Solidity=0.5

Fig. 10: Normal and tangential force components for different solidities of S809 airfoil.

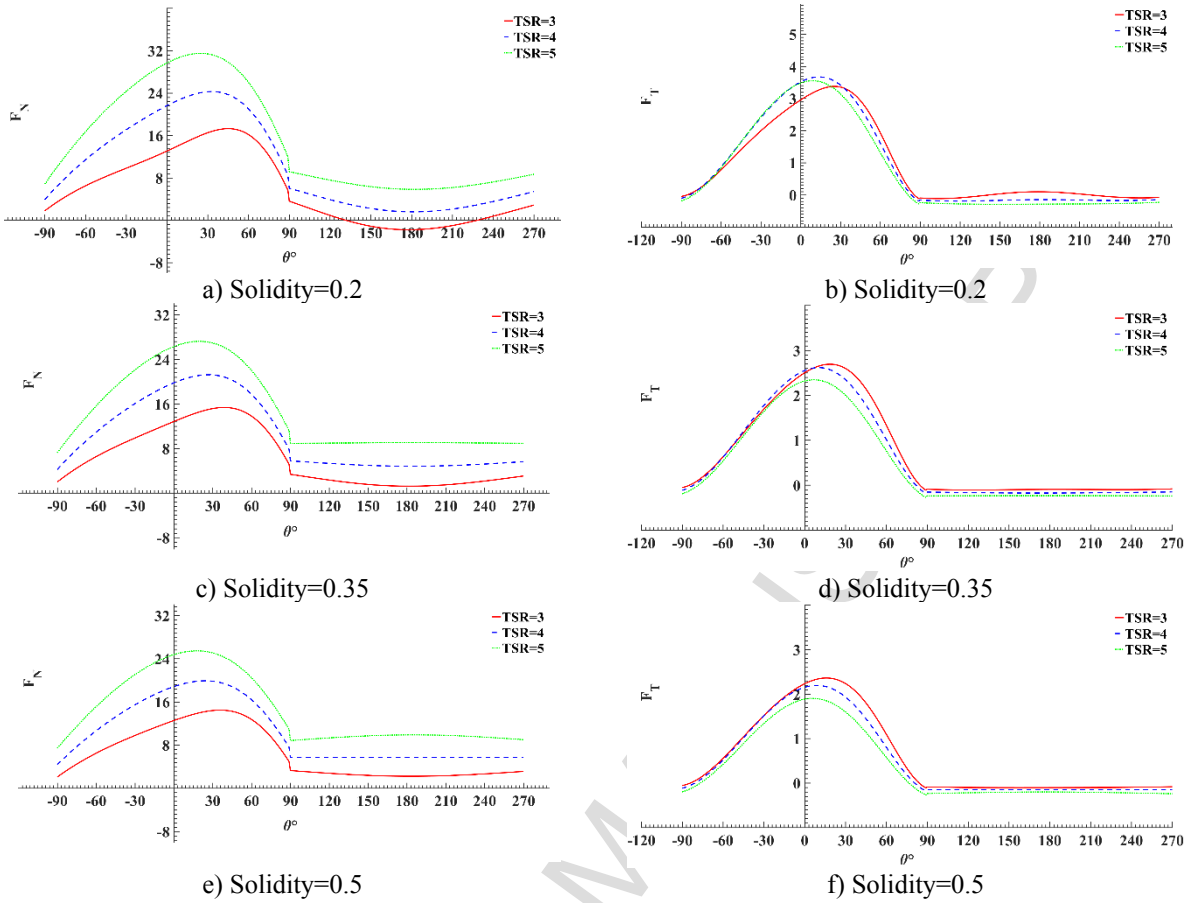

a) Solidity=0.2 b) Solidity=0.2

c) Solidity=0.35 d) Solidity=0.35

e) Solidity=0.5 f) Solidity=0.5

Fig. 11: Normal and tangential force components for different solidities of S814 airfoil.

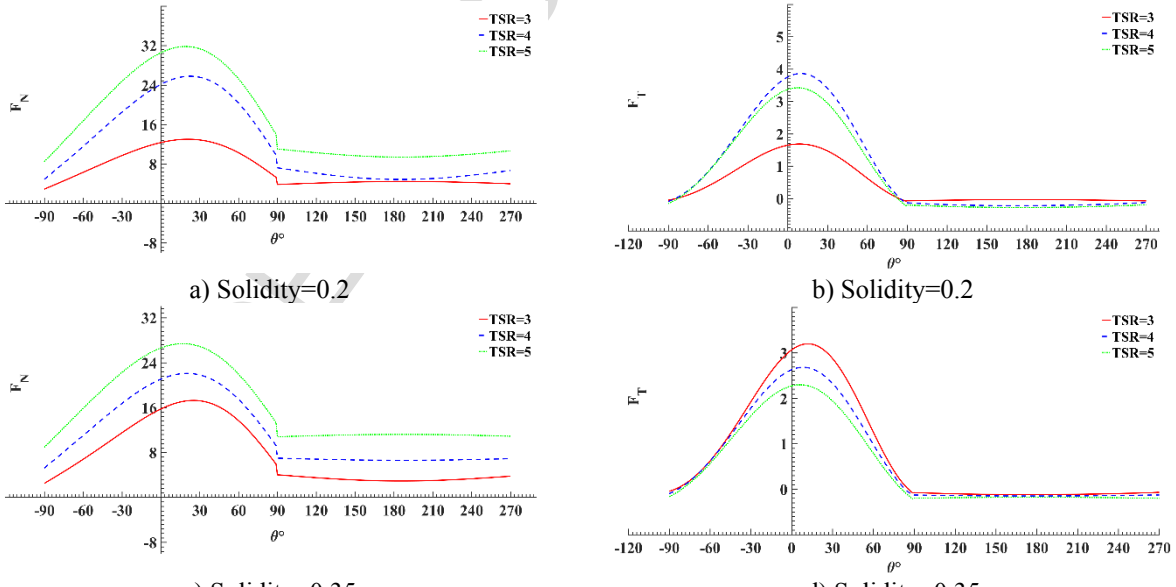

a) Solidity=0.2 b) Solidity=0.2

c) Solidity=0.35 d) Solidity=0.35

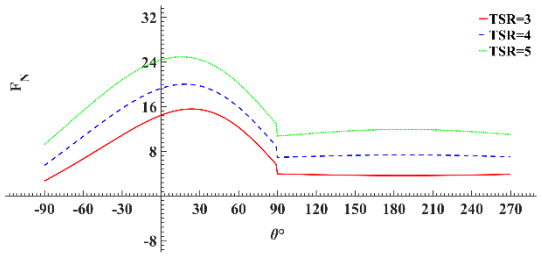

e) Solidity=0.5

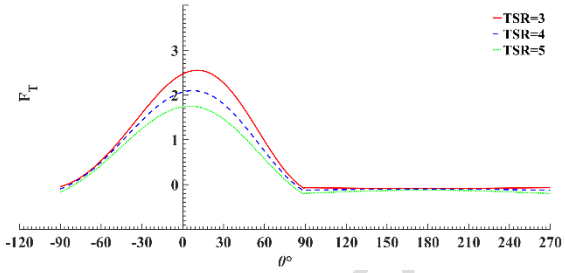

f) Solidity=0.5

Fig. 12: Normal and tangential force components for different solidities of RISØ-A1-24 airfoil.

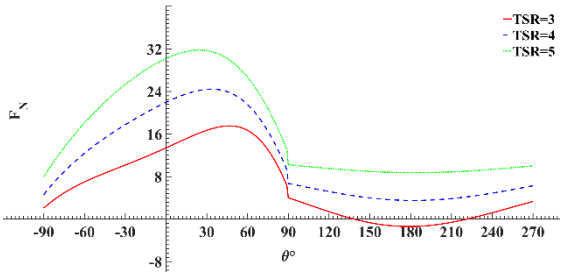

a) Solidity=0.2

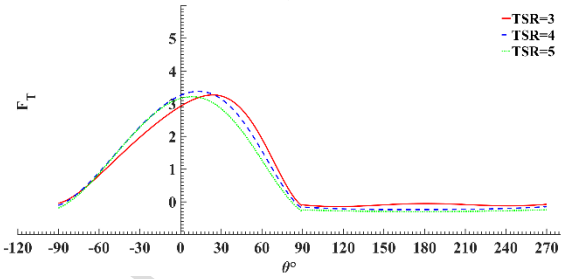

b) Solidity=0.2

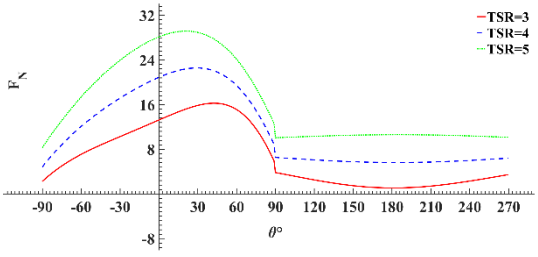

c) Solidity=0.35

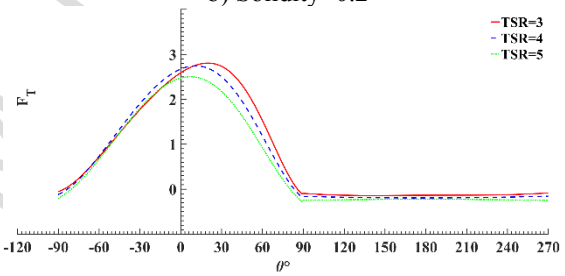

d) Solidity=0.35

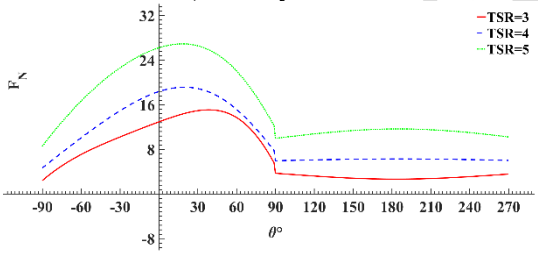

e) Solidity=0.5

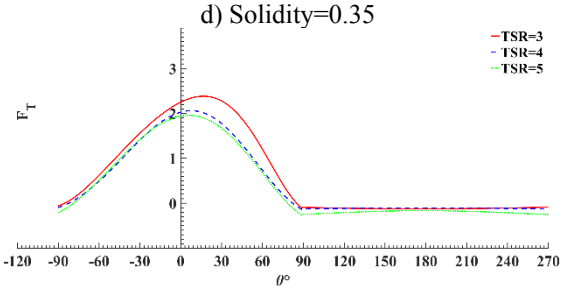

f) Solidity=0.5

Fig. 13: Normal and tangential force components for different solidities of DU 93-W-210 airfoil.

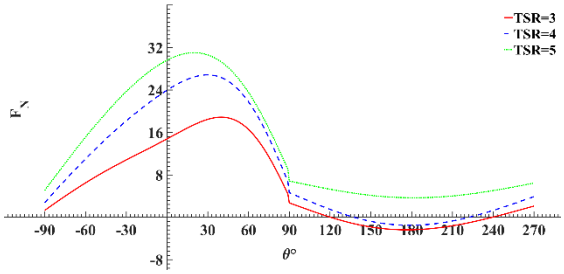

a) Solidity=0.2

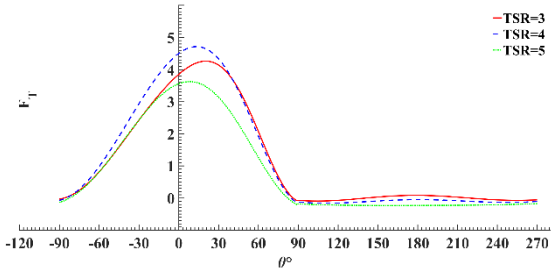

b) Solidity=0.2

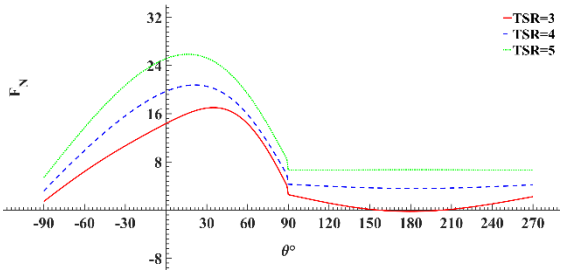

c) Solidity=0.35

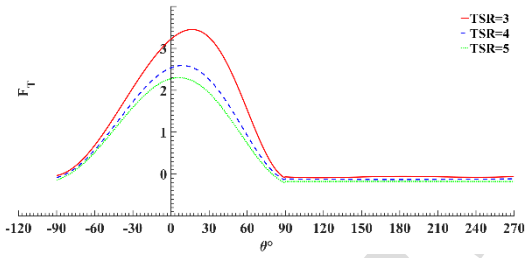

d) Solidity=0.35

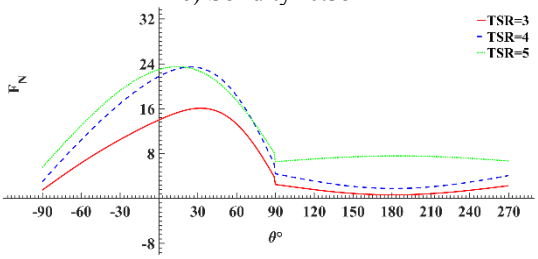

e) Solidity=0.5

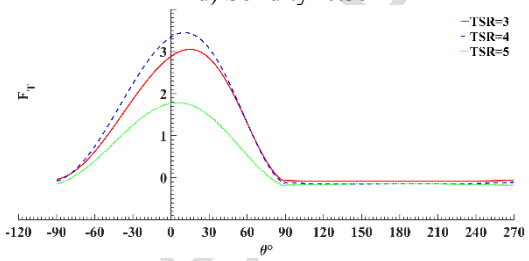

f) Solidity=0.5

1 **Fig. 14:** Normal and tangential force components for different solidities of FFA-W3-241 airfoil.

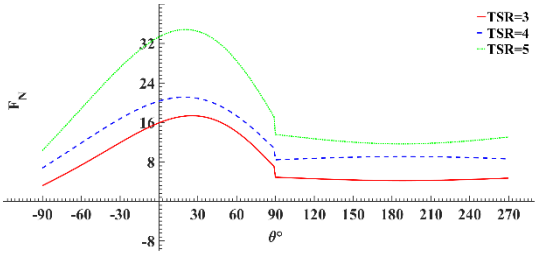

a) Solidity=0.2

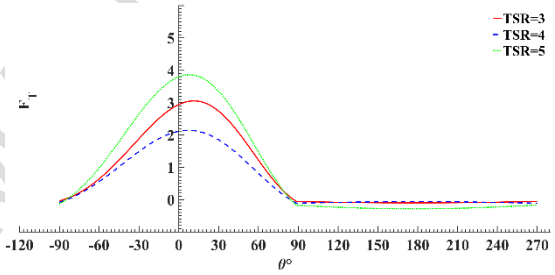

b) Solidity=0.2

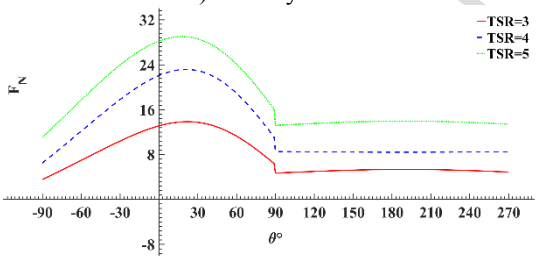

c) Solidity=0.35

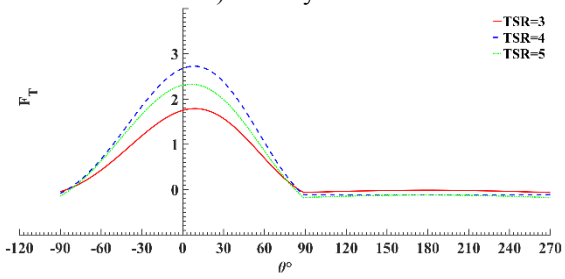

d) Solidity=0.35

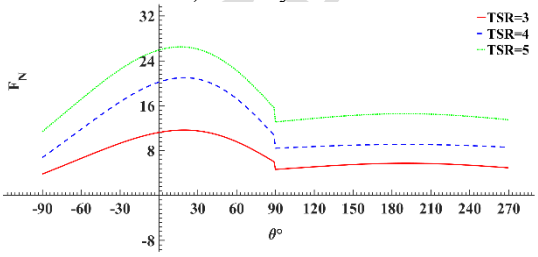

e) Solidity=0.5

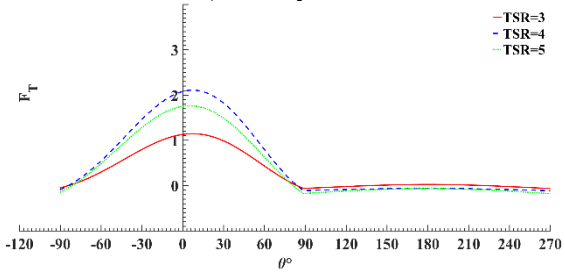

f) Solidity=0.5

2 **Fig. 15:** Normal and tangential force components for different solidities of FX66-S196-V1 airfoil.

3

6.2 Power generation

When the rotor blade is located in the upstream region, power coefficient increases, reaching its maximum at zero azimuth angle. In contrast, when the wind turbine passes through the downstream region, power coefficient will be reduced. This phenomenon appears in all tip-speed ratios during the rotor rotation, so the upstream region is extremely important for power generation using VAWTs. In this study, the rated wind speed was considered to be12 m/s for all airfoils. In Fig. 16, power generation of different airfoils is plotted for Cp_{max} at rated wind speed of 12 m/s. Statistical analysis can be used to calculate the potential wind energy output for a given site. To estimate the annual energy production for the designed wind turbines, a Gaussian function such as the one shown in Equation 15 was fitted with a plot of power production versus wind speed (see Fig. 16). The Gaussian function was fitted with the power productions of each airfoil, and the constants shown in Eq. 15 are summarized for all airfoils in Table 4. According to the literature [38], the Weibull distribution is the most common distribution that is used to accurately describe wind frequency, and it is useful for extracting the annual energy production for a given wind turbine. The Weibull probability density function is shown by Eq. 16 [1], in which k and c are the shape and scale factors also given in Table 2 at heights of 10 m and 40 m for the Khaf area. The annual energy production was calculated using Eq. 17, in which N is the number of wind speed measurements in a year, i.e., 52,560, and $\Delta t = \frac{1}{6}$ h. The data collection interval was reported as 10 min for this set of wind data from the Khaf area. As shown in Fig. 17, two airfoils of RISØ-A1-24 and FFA-W3-241 produced the greatest annual energy production when compared to the other airfoils. According to this figure, for the height of 10 m, the minimum and maximum annual energy production values are 12.59 MWh (S809) and 15.41 MWh (FFA-W3-241), respectively. For a height of 40 m, corresponding values are 13.47 MWh (S809) and 16.42 MWh (FFA-W3-241), respectively. Therefore, results for annual energy production indicate that airfoil selection is one of the most effective parameters in generating more annual power while other design parameters are fixed. In Table 5, the annual energy production of all airfoils is summarized for heights of 10 m and 40 m.

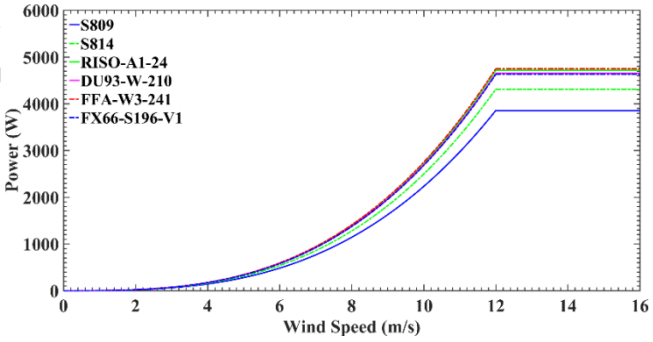

Fig. 16: Comparison of power production vs wind speed for all airfoils.

$$Power(U) = a_1 \exp(-(\frac{U-b_1}{c_1})^2) + a_2 \exp(-(\frac{U-b_2}{c_2})^2) + a_3 \exp(-(\frac{U-b_3}{c_3})^2) + a_4 \exp(-(\frac{U-b_4}{c_4})^2) \quad (15)$$

$$f(U) = \left(\frac{k}{c}\right)\left(\frac{U}{c}\right)^{k-1} \exp\left[-\left(\frac{U}{c}\right)^{k}\right] \quad (16)$$

$$\overline{P}_{Total} = \left(\int_0^{\infty} Power(U) f(U) dU\right) \times N \times \Delta t \quad (17)$$

1

Table 4
Constant coefficients of Gaussian curve fitting function.

Airfoil	a_1	b_1	c_1	a_2	b_2	c_2	$a_3 \times 10^5$	b_3	c_3	$a_4 \times 10^5$	b_4	c_4
S809	2016	11.57	4.633	4436	14.69	3.053	1.58	14.22	1.263	-1.59	14.22	1.268
S814	2254	11.56	4.631	4964	14.69	3.054	1.76	14.22	1.262	-1.78	14.22	1.268
RISØ24	2470	11.57	4.635	5422	14.69	3.051	1.93	14.22	1.263	-1.95	14.22	1.268
DU93	2428	11.56	4.631	5351	14.69	3.055	1.91	14.22	1.262	-1.93	14.22	1.268
FFA	2772	11.97	4.785	5305	14.68	2.892	1.07	14.22	1.276	-1.11	14.23	1.288
FX66	2418	11.56	4.631	5330	14.69	3.055	1.89	14.22	1.262	-1.92	14.22	1.268

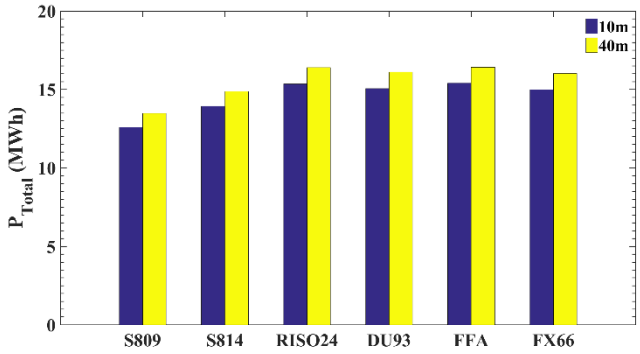

Fig. 17: Comparison of annual energy production of different airfoils at heights of 10 m and 40 m.

2 **6.3 Economical evaluation**

3 Wind energy is one of the most appropriate sources of clean energy, thereby increasing the importance of
4 designing wind turbines with high performance that use inexpensive manufacturing methods. As a result,
5 wind turbine designers should consider the costs of improvement in aerodynamic performance. Over the
6 past several decades, certain developments in wind turbine technology changed the price levels of
7 designing wind turbines from 5000 $US/kW to 1000 $US/kW [41], making wind energy the most
8 profitable resource among other energy resources. In this section, economic evaluation is carried out for
9 different airfoil profiles to compare the resulting costs of each airfoil section if no other parameters are
10 changed. This comparison shows that wind turbine companies and investors in wind energy, especially

the VAWT type, achieve a huge profit by changing only the airfoil section, while other design parameters are fixed. The annual operation and maintenance costs in the first year can be calculated using Eq. 18 [1].

$$C_{OM} = mC_I \tag{18}$$

where C_I is the initial investment of the project, C_{OM} is the operation and maintenance cost, and m is the ratio of C_{OM}/ C_I. The following equation provides an estimate of the maintenance and operational cost for a wind turbine life span of n years compared to the initial year.

$$PW(C_{OM})_{1-n} = mC_I\left[\frac{(1+I)^n - 1}{I(1+I)^n}\right] \tag{19}$$

where I is the annual interest rate, which is different for each country. The annual interest rate for Iran was reported by the National Central Bank of Iran [42] as 20%. Eqs. 20 and 21 define the net present worth of all costs, including operation, maintenance, and the initial investment.

$$NPW(C_A)_{1-n} = C_I\left[1 + m\left(\frac{(1+I)^n - 1}{I(1+I)^n}\right)\right] \tag{20}$$

which results in annual cost of the turbine operation as follows:

$$NPW(C_A) = \frac{NPW(C_A)_{1-n}}{n} = \frac{C_I}{n}\left[1 + m\left(\frac{(1+I)^n - 1}{I(1+I)^n}\right)\right] \tag{21}$$

The annual output energy production by the turbine can be derived as follows:

$$E_I = 8760 \times P_R \times CF \tag{22}$$

where P_R is the rated power and CF is the capacity factor of the wind turbine. The following equation calculates the capacity factor of the wind turbine, defined as the ratio of actual generated power to the rated power output.

$$\text{Capacity Factor(CF)} = \frac{\overline{P}_{Total}\text{MWh}}{(365\text{days}) \times (24\text{h/day}) \times (P_R\text{kW}) \times 1\text{MW}/1000\text{kW}} \tag{23}$$

Finally, the cost of 1kWh electricity (C) generated by the wind turbine is defined by:

$$C = \frac{NPW(C_A)}{E_I} = \frac{C_I}{8760n}\left(\frac{1}{P_R CF}\right)\left[1 + m\left(\frac{(1+I)^n - 1}{I(1+I)^n}\right)\right] \quad (24)$$

To calculate the cost of 1 kWh of electricity for the current H-type VAWT with different airfoil sections, following assumptions were made:

1) Design cost of the wind turbine is 1000 $/kW (based on the manufacturing price in Iran).
2) Other costs, including installation, transportation, custom-free status, and grid integration, are considered to be 40% of the turbine production cost [43].
3) Annual operation and maintenance costs plus land rental are about 6% (m=0.06) of the turbine production cost [43].
4) Life of the wind turbine is 15 years (n=15) [43].
5) Interest rate is 20% for each year over the 15-year period (I=0.2).
6) Capacity factor of the wind turbine was calculated for heights of 10 m and 40 m (Table 5).
7) Initial investment (C_I) and installation costs (IC) were calculated as follows:

Installation cost (IC) = Rated power (kW)×1000($/kW)×$\frac{40}{100}$

Total initial investment (C_I) = Rated power (kW)×1000($/kW) + Installation cost (IC)

In Fig. 18, a bar graph of the total cost for 1 kWh of wind-generated electricity is plotted for different airfoils at heights of 10 m and 40 m. As shown in Fig. 18, total cost of electricity generation is greater at a height of 10 m than at 40 m. In Table 5, a complete summary of the economic evaluation, including annual energy ($\overline{P}_{Total}$), capacity factor (CF), and total cost (C) is reported for heights of 10 m and 40 m for different airfoils, and the installation cost (IC) and total initial investment (C_I) are calculated for all airfoils in Table 5. For a height of 10 m, the minimum cost is associated with the S809 airfoil (0.0365 $/kWh), and the maximum cost is associated with the S814 airfoil (0.0370 $/kWh). For a height of 40 m, the minimum cost is associated with the S809 airfoil (0.0342 $/kWh), and the maximum cost is associated with the S814 and FFA-W3-241 airfoils (0.0346 $/kWh). According to these results, total cost (C) at height of 10 m is roughly 7% more than the height of 40 m, a significant difference for total investment of this size. Conversely, the annual energy production ($\overline{P}_{Total}$) at height of 40 m is approximately 7% more than that at height of 10 m, so the results indicate that designing a H-type VAWT with greater height is more economical and productive than the one with a lower height. To examine the effect of airfoil selection, a comparison of total costs shows that differences between costs of the energy generation for

various airfoils are not significant. While the total cost of the generation of electrical energy for all profiles are about equal, a comparison between annual energy production at different heights indicates that, for height of 40 m, the maximum annual energy (16.42 MWh) produced by FFA-W3-241 airfoil is 22% more than for the smallest value of annual energy, that occurred for the S809 airfoil (13.47 MWh). In general, although changing the airfoil profile does not have a substantial effect on total investment costs; it has a definite influence on annual power production. According to Table 5, the most effective and economic airfoil section is the FFA-W3-241 airfoil. Since the price level for selling power from the wind turbine is currently 0.15 $/kWh in Iran, designing this H-rotor VAWT with airfoil FFA-W3-241 would be an extremely beneficial investment because the selling price level (0.15 $/kWh) is 4.33 times the total investment cost (0.0346 $/kWh) in the Khaf area.

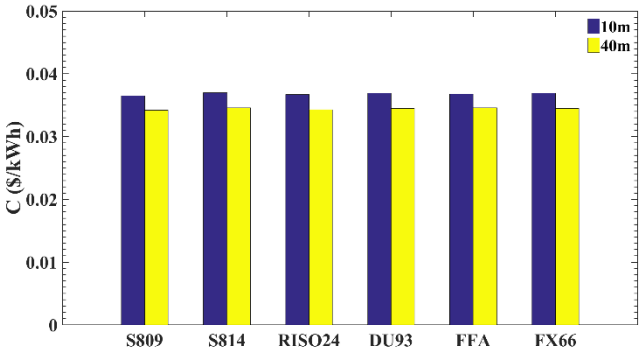

Fig. 18: Cost of 1 kWh wind-generated electricity for different airfoils at heights of 10 m and 40 m.

Table 5
Energy production and economical evaluation for H-type VAWT designed for Khaf area (Iran).

Airfoil type	$\overline{P}_{Total}$ (MWh)	CF	C ($/kWh)	$\overline{P}_{Total}$ (MWh)	CF	C ($/kWh)	IC ($)	TI ($)
	10 m			40 m				
S809	12.59	0.3733	0.0365	13.47	0.3992	0.0342	1540	5390
S814	13.94	0.3692	0.0370	14.89	0.3944	0.0346	1724	6034
RISØ-A1-24	15.36	0.3722	0.0367	16.41	0.3978	0.0343	1884	6594
DU 93-W-210	15.07	0.3700	0.0369	16.12	0.3954	0.0345	1860	6510
FFA-W3-241	15.41	0.3702	0.0368	16.42	0.3945	0.0346	1900	6650
FX66-S196-V1	15.00	0.3700	0.0369	16.03	0.3953	0.0345	1852	6482

7. Conclusions

In the current study, the DMST model was used to analyze the aerodynamic performance of a vertical axis wind turbine with H-type rotor configuration. To study the effect of different airfoil profiles on power generation and total investment cost, six different airfoils (S809, S814, RISØ-A1-24, DU 93-W-210, FFA-W3-241, and FX66-S196-V1) were compared. The examination was performed for different

solidity values ranging from 0.2 to 0.6, and 12 different tip-speed ratios ranging from 1 to 12, while blade height, chord length, and number of blades were kept constant. Comparison of the power coefficient for different solidities from 0.2 to 0.6 and tip-speed ratios demonstrated that there is an optimum solidity to extract the maximum power from wind turbine and it was found 0.5 for the present studied airfoils. Comparison of tangential forces demonstrated that the effect of changing solidity and tip-speed ratio is significant in some cases, including RISØ-A1-24, FFA-W3-241, and FX66-S196-V1, but was found to be insignificant in some other cases such as S809, S814, and DU 93-W-210. Airfoil FFA-W3-241 produced the maximum tangential force at tip-speed ratio of 3 or 4, and for different solidities. RISØ-A1-24 and FFA-W3-241 airfoil produced the most annual energy compared to the other airfoils. At the height of 10 m, the minimum and maximum annual energy productions were 12.59 MWh (S809) and 15.41 MWh (FFA-W3-241), respectively. At a height of 40 m, the minimum and maximum annual energy productions were 13.47 MWh (S809) and 16.42 MWh (FFA-W3-241), respectively. Therefore, the results of the annual energy production analysis indicate that airfoil selection is an effective step in design process related to greater annual power generation while other design parameters are fixed. In general, although changing the airfoil profile has insignificant effect on the total investment cost, it has a great influence on annual power production. The most effective and economic airfoil section was found to be FFA-W3-241. Since the sale price of electrical power is currently 0.15 $/kWh in Iran, choosing the FFA-W3-241 airfoil for the current H-rotor VAWT would be significantly profitable, since it is 4.33 (0.15/0.0346) times the of the total investment cost (0.0346 $/kWh) in the Khaf area.

References

[1] Saeidi D, Sedaghat A, Alamdari P, Alemrajabi AA. Aerodynamic design and economical evaluation of site specific small vertical axis wind turbines. Appl. Energy 2013; 101:765-775.

[2] U.S. Energy Information Administration. Prediction of world energy consumption by 2040. https://www.eia.gov/todayinenergy/detail.php?id=32912 [accessed 20 October 2017].

[3] Chizfahm A, Yazdi EA, Eghtesad M. Dynamic modeling of vortex induced vibration wind turbines. Renewable Energy. 2018;121:632-43.

[4] Qamar SB, Janajreh I. A comprehensive analysis of solidity for cambered darrieus VAWTs. International Journal of Hydrogen Energy. 2017; 42(30):19420-31.

[5] Ghasemian M, Ashrafi ZN, Sedaghat A. A review on computational fluid dynamic simulation techniques for Darrieus vertical axis wind turbines. Energy Conversion and Management. 2017; 149:87-100.

[6] Chaichana T, Chaitep S. Wind power potential and characteristic analysis of Chiang Mai, Thailand. J Mech Sci Technol. 2010; 24:1475-1479.

[7] Tjiu W, Marnoto T, Mat S, Ruslan MH. Darrieus vertical axis wind turbine for power generation I: Assessment of Darrieus VAWT configurations. Renew Energy 2015; 75:50-67.

[8] Singh MA, Biswas A, Misra RD. Investigation of self-starting and high rotor solidity on the performance of a three S1210 blade H-type Darrieus rotor. Renew Energy 2015; 76:381-387.

[9] Sutherland HJ, Berg DE, Ashwill, TD, A retrospective of VAWT technology. Tech. rep., Sandia National Laboratories Report SAND2012-0304. 2012.

[10] Li Q, Maeda T, Kamada Y, Murata J, Shimizu K, Ogasawara T, Nakai A, Kasuya T. Effect of solidity on aerodynamic forces around straight-bladed vertical axis wind turbine by wind tunnel experiment (depending on number of blades). Renew. Energy 2016; 96:928-939.

[11] Bachant P, Wosnik M. Characterising the near-wake of a cross-flow turbine. J Turbul. 2015; 16: 392–410.

[12] Klimas P, Worstell M. Effects of blade preset pitch/offset on curved-blade Darrieus vertical axis wind turbine performance. Sandia National Laboratory Report. Sand-18-1762. Albuquerque NM, 1981.

[13] Brochier G, Fraunie P, Beguier C, Paraschivoiu I. Water channel experiments of dynamic stall on Darrieus wind turbine blades. AIAA J Propul Power. 1986; 2: 445–449.

[14] Battisti L, Zanne L, Dell'Anna S, Dossena V, Persico G, Paradisuo B. Aerodynamic measurements on a vertical axis wind turbine in a large scale wind tunnel. J Energy Resour Technol. 2011; 133(3):031201.

[15] Posa A, Parker CM, Leftwich MC, Balaras E. Wake structure of a single vertical axis wind turbine. International Journal of Heat and Fluid Flow. 2016; 61(Part A):75-84.

[16] Shamsoddin S, Porté-Agel F. Large eddy simulation of vertical axis wind turbine wakes. Energies. 2014; 7: 890–912.

[17] Shamsoddin S, Porté-Agel F. A large-eddy simulation study of vertical axis wind turbine wakes in the atmospheric boundary layer. Energies. 2016; 9(5):366.

[18] Subramanian A, Yogesh SA, Sivanandan H, Giri A, Vasudevan M, Mugundhan V, Velamati RK. Effect of airfoil and solidity on performance of small scale vertical axis wind turbine using three dimensional CFD model. Energy 2017; 133:179-190.

[19] Brulle RV. Feasibiliy investigation of the giromill for generation of electrical power. Technical discussion, vol. li. Energy Research and Development Administration; 1977. COO/2617-76/1/2.

[20] Mohamed MH. Performance investigation of H-rotor Darrieus turbine with new airfoil shapes. Energy 2012; 47; 522-530.

[21] Sengupta AR, Biswas A, Gupta R. Studies of some high solidity symmetrical and unsymmetrical blade H-Darrieus rotors with respect to starting characteristics, dynamic performances and flow physics in low wind streams. Renewable Energy 2016; 93: 536-547.

[22] Chen J, Chen L, Xu X, Yang H, Ye C, Liu D. Performance improvement of a vertical axis wind turbine by comprehensive assessment of an airfoil family. Energy 2016; 114: 318-331.

[23] Ma N, Lei H, Han Z, Zhou D, Bao Y, Zhang K, Zhou L, Chen C. Airfoil optimization to improve power performance of a high-solidity vertical axis wind turbine at a moderate tip speed ratio. Energy. 2018 ;150:236-52.

[24] Bukala J, Damaziak K, Karimi HR, Kroszczynski K, Krzeszowiec M, Malachowski J. Modern small wind turbine design solutions comparison in terms of estimated cost to energy output ratio. Renewable Energy. 2015;83:1166-73.

[25] Wiser R, Bolinger M. 2010 Wind technologies market report. National Renewable Energy Lab. (NREL), Golden, CO (United States); 2011.

[26] Cleantechnica (2011), Cost of Wind Power-Kicks coal's butt better than Natural gas, May, http://cleantechnica.com/2011/05/01/cost-of-wind-power-kicks-coals-butt-better-than- natural-gas-could-power-your-ev-for-0-70gallon)

[27] https://www.eia.gov

[28] Templin RJ. Aerodynamic performance theory for the NRC vertical-axis wind turbine. NRC Lab. Report; 1974.

[29] Paraschivoiu I. Wind turbine design: with emphasis on Darrieus concept. Canada: Polytechn Int Press; 2002. ISBN 2-553-00931-3

[30] Coiro DP, De Marco A, Nicolosi F, Melone S, Montella F. Dynamic behaviour of the patented kobold tidal current turbine: numerical and experimental aspects. Acta Polytechnica. 2005;45(3):77-84.

[31] Ahmadi-Baloutaki M. Analysis and Improvement of Aerodynamic Performance of Straight Bladed Vertical Axis Wind Turbines. PhD Dissertation, University of Windsor, 2015.

[32] Scheurich F., Fletcher TM., Brown RE., Effect of blade geometry on the aerodynamic loads produced by vertical-axis wind turbines, Proceedings of the Institution of Mechanical Engineers, Part A: Journal of Power and Energy, 2011; 225:327-341.

[33] Ahmadi-Baloutaki M, Carriveau R, Ting DS. Straight-bladed vertical axis wind turbine rotor design guide based on aerodynamic performance and loading analysis. Proceedings of the Institution of Mechanical Engineers, Part A: Journal of Power and Energy. 2014;228(7):742-59.

[34] Paraschivoiu I. Double-multiple stream tube model for Darrieus wind turbine. In: Second DOE/NASA wind turbine dynamics workshop, NASA CP-2186, Cleveland, OH; 1981. P. 10-25.

[35] Bertagnolio F, Sorensen N, Johansen J, Fuglsang P. Wind turbine airfoil catalogue. Risø-R-1280 (EN). Roskilde, Denmark: Risø National Laboratory; 2001.

[36] Islam M, Ting DSK, Fartaj A. Aerodynamic models for Darrieus-type straight-bladed vertical axis wind turbines. Renew Sustain Energy Rev 2008; 12; 1087-109.

[37] Blackwell BF, Sheldahl RE, Feltz LV. Wind tunnel performance data for the Darrieus wind turbine with NACA 0012 blades. SAND76-0130 Sandia Labs. (USA); 1976 May 1.

[38] Alamdari P, Nematollahi O, Mirhosseini M. Assessment of wind energy in Iran: A review. Renew Sustain Energy Rev. 2012;16(1):836-60.

[39] Li C, Zhu S, Xu YL, Xiao Y. 2.5 D large eddy simulation of vertical axis wind turbine in consideration of high angle of attack flow. Renewable energy. 2013;51:317-30.

[40] Paraschivoiu I. Predicted and experimental aerodynamic forces on the Darrieus rotor. Journal of energy. 1983;7(6):610-5.

[41] Hau E. Wind Turbine Fundamentals, Technologies, Application, Economics. 2nd ed. Berlin. Spring. 2006.

[42] Bank Meli Iran. http://www.bmi.ir/ [accessed 20 October 2017].

[43] Mostafaeipour A, Sedaghat A, Dehghan-Niri AA, Kalantar V. Wind energy feasibility study for city of Shahrbabak in Iran. Renew Sustain Energy Rev 2011;15:2545–56.

Appendix

C_D/C_L versus azimuth angle is plotted here for all the airfoils at λ =3, 4, and 5, while σ = 0.2 to 0.5. The results generally show that the maximum peak of angle of attack is reduced by an increase in the tip-speed ratio. For all airfoil sections, the highest angle of attack varies between 5º and 15° depending on the tip-speed ratio and the solidity. The lift coefficient increases with rising λ and the drag coefficient is increased with the tip-speed ratio. Although they have a similar tendency, the ratio of drag coefficient to lift coefficient exhibits a different trend. According to the C_D/C_L, results there is a significant peak for C_D/C_L at an azimuth angle of 0° for some airfoil sections, including S809, S814, DU 93-W-210, particularly for λ=3. Conversely, there is no obvious peak and also no such difference for other airfoil sections, including FFA-W3-241, RISØ-A1-24 and FX66-S196-V1.

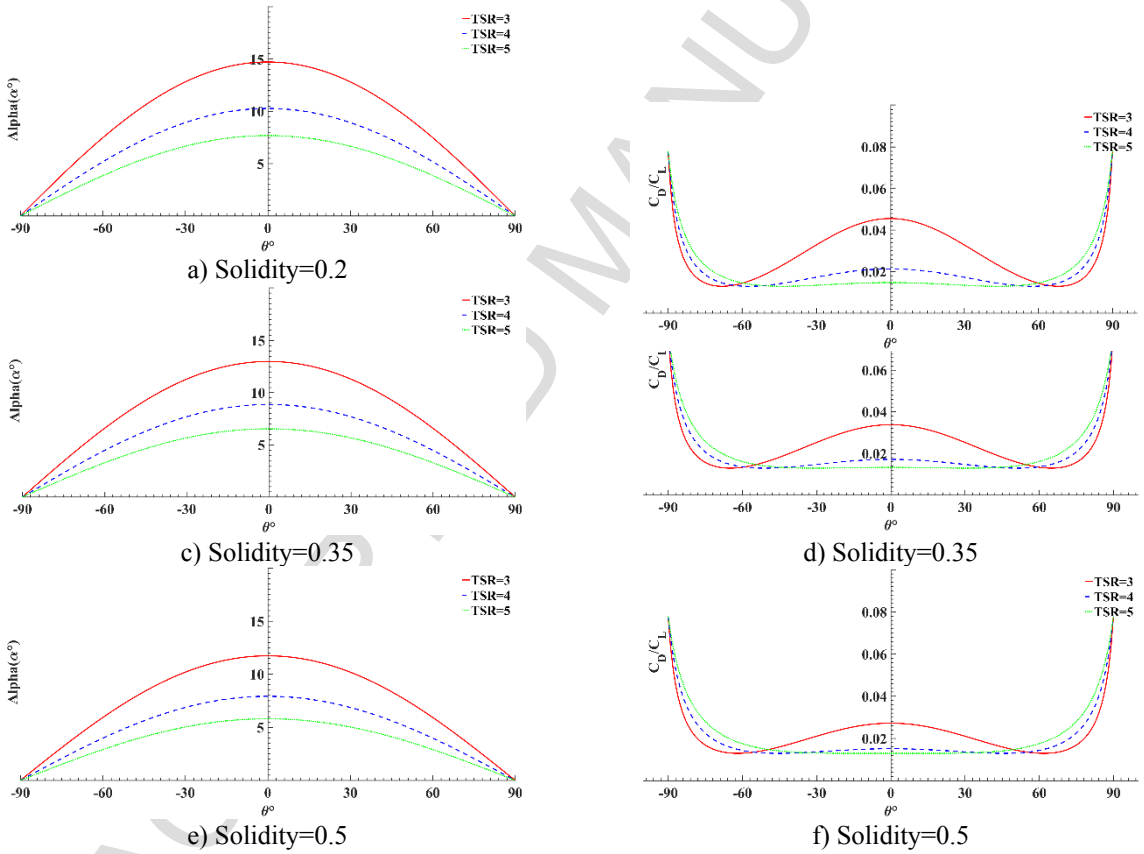

Fig. A1: Angle of attack and C_D/C_L vs tip speed ratio for different solidities of S809 airfoil.

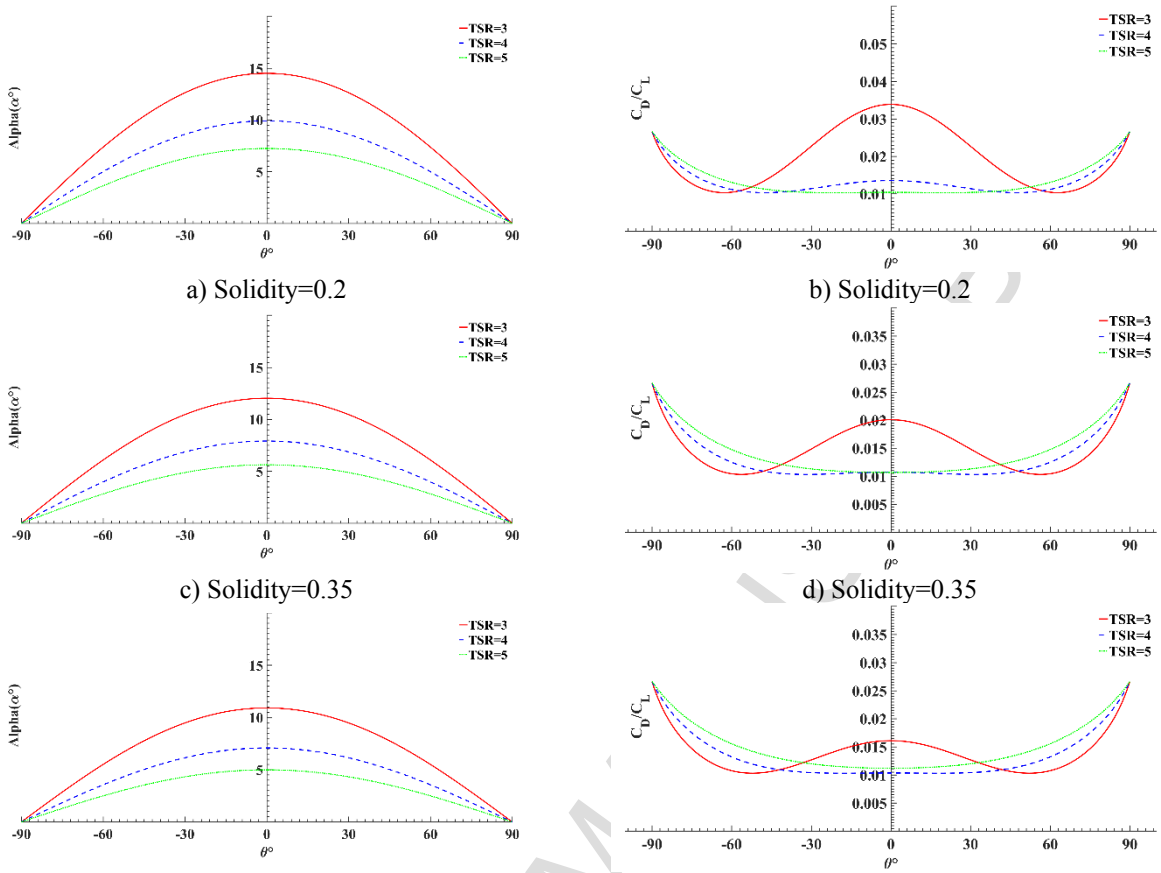

a) Solidity=0.2 b) Solidity=0.2

c) Solidity=0.35 d) Solidity=0.35

e) Solidity=0.5 f) Solidity=0.5

Fig. A2: Angle of attack and C_D/C_L vs tip speed ratio for different solidities of S814 airfoil.

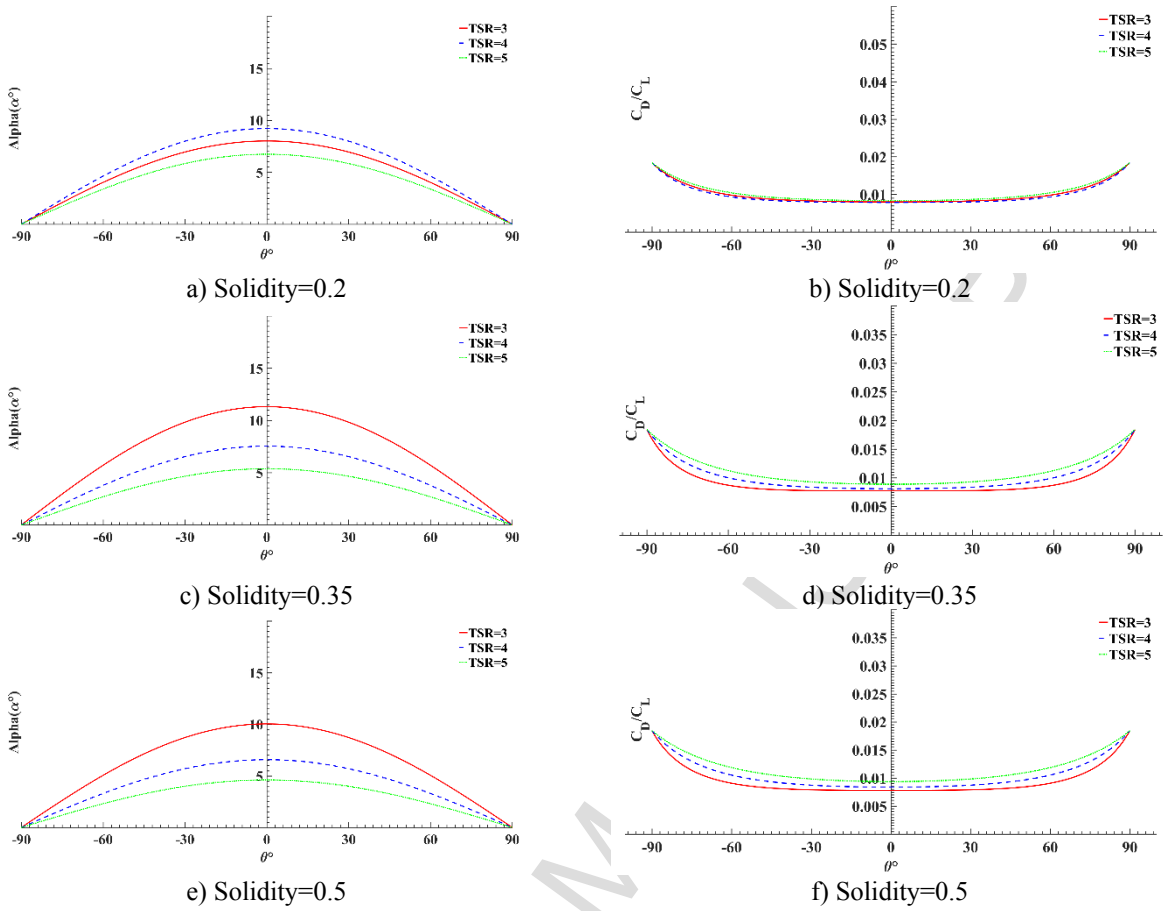

a) Solidity=0.2 b) Solidity=0.2

c) Solidity=0.35 d) Solidity=0.35

e) Solidity=0.5 f) Solidity=0.5

Fig. A3: Angle of attack and C_D/C_L vs tip speed ratio for different solidities of RISØ-A1-24 airfoil.

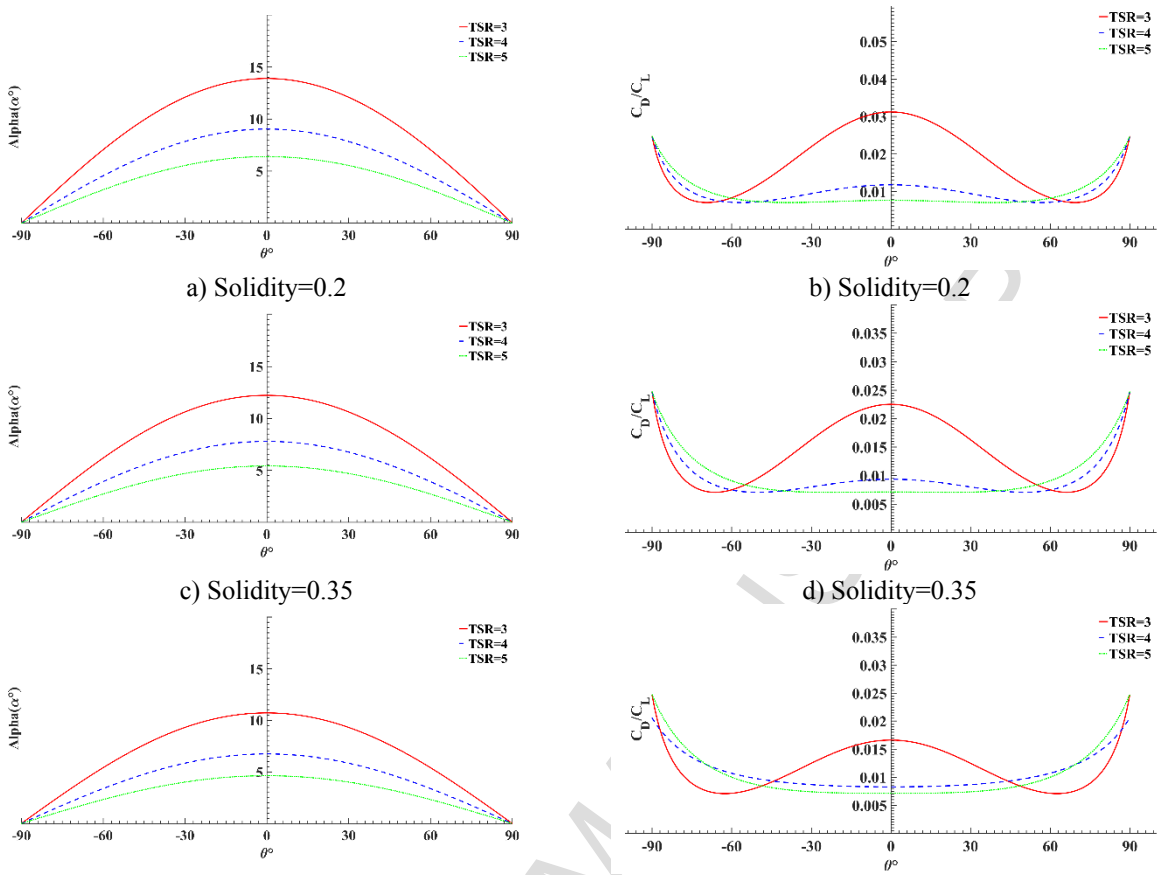

a) Solidity=0.2 b) Solidity=0.2

c) Solidity=0.35 d) Solidity=0.35

e) Solidity=0.5 f) Solidity=0.5

Fig. A4: Angle of attack and C_D/C_L vs tip speed ratio for different solidities of DU 93-W-210 airfoil.

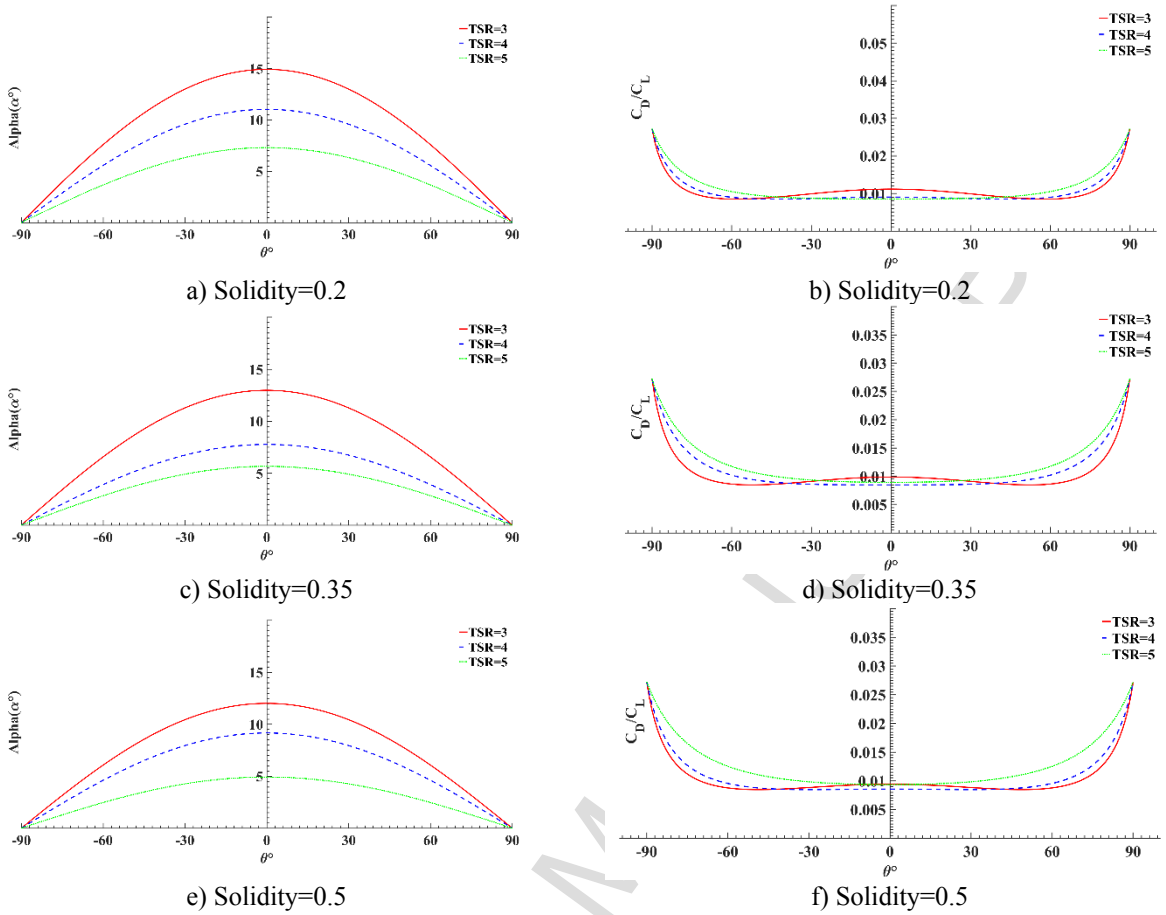

a) Solidity=0.2 b) Solidity=0.2

c) Solidity=0.35 d) Solidity=0.35

e) Solidity=0.5 f) Solidity=0.5

Fig. A5: Angle of attack and C_D/C_L vs tip speed ratio for different solidities of FFA-W3-241 airfoil.

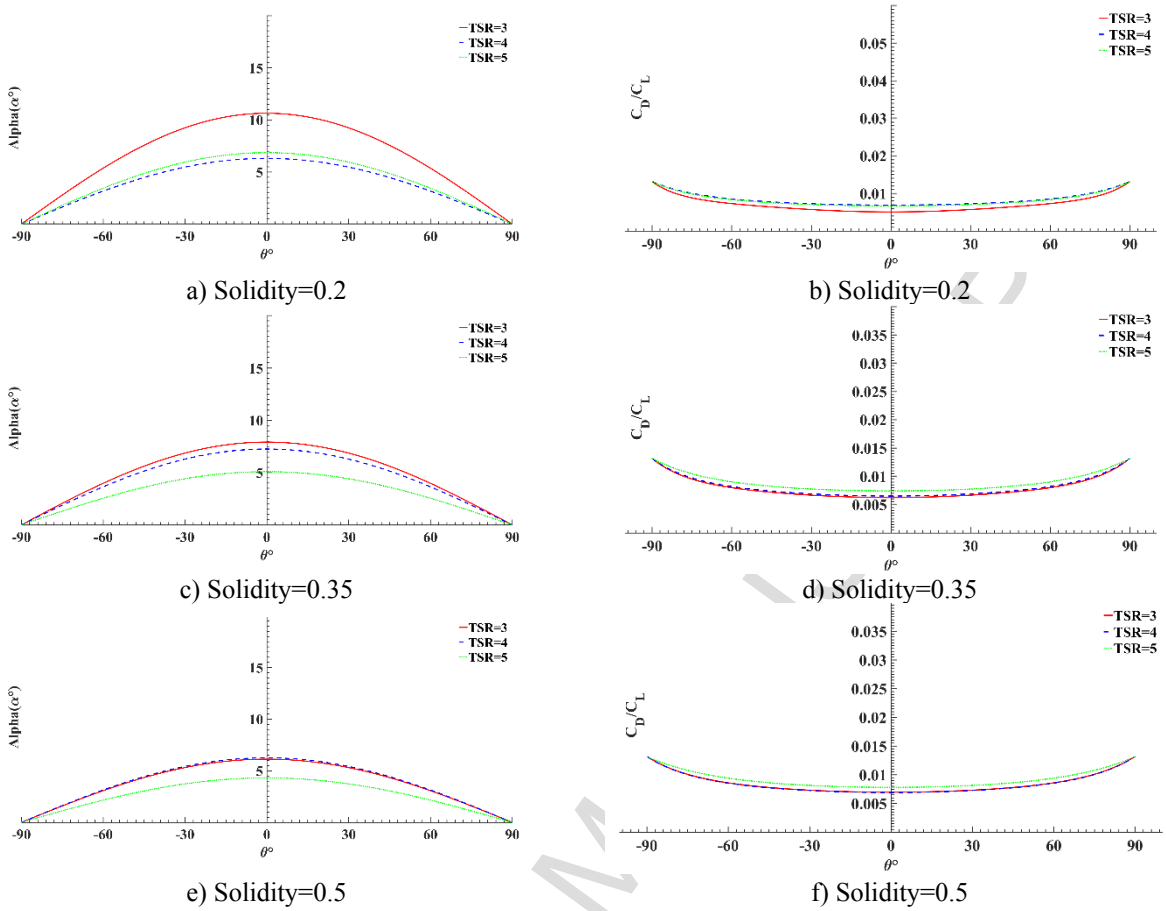

a) Solidity=0.2 b) Solidity=0.2

c) Solidity=0.35 d) Solidity=0.35

e) Solidity=0.5 f) Solidity=0.5

1 **Fig. A6:** Angle of attack and C_D/C_L vs tip speed ratio for different solidities of FX66-S196-V1 airfoil.

2

Research Highlights

- Predicting aerodynamic performance of H-type VAWTs using DMST and BEM methods.
- Aerodynamic and economic evaluation of asymmetric HAWT's airfoils for VAWTs.
- Evaluation of force components at different solidities and tip speed ratios.